Observations of a barotropic planetary wave in the western North Atlantic

by James F. Price[1] and H. Thomas Rossby[2]

ABSTRACT

SOFAR float observations from 1300 m depth are used to describe a major feature of the large-scale, subthermocline velocity field observed in the western North Atlantic (31N, 70W), during the 1978 POLYMODE Local Dynamics Experiment (LDE). The two-month-long intensive phase of the LDE was dominated by a highly polarized, oscillatory flow which had many of the characteristics of a barotropic planetary wave. Space- and time-lagged covariance analyses indicate that phase propagated toward 300°T, the estimated wave vector direction, at 0.06 ms^{-1}. The wavelength and intrinsic period are estimated to be 340 km and 61 days, which are consistent with the dispersion relation for barotropic planetary waves modified by topography. Group velocity inferred from the dispersion relation was eastward.

The observed velocity followed barotropic potential vorticity conservation to within estimated error, $\cong$ 15% of R, the relative vorticity. R oscillated between $\pm$ 4% of f, the Coriolis parameter, as fluid columns oscillated northeast to southwest through a similar range of ambient vorticity. The beta effect and topographic stretching acted in phase, and were of comparable magnitude.

The wave was temporally intermittent. It accounts for 77% of the variance of the observed, large-scale velocity during the first 90 days of the LDE, but accounts for essentially none of the variance during the second 90 days when the observed velocity was much weaker and less polarized.

1. Introduction

Here we describe an energetic, large-scale, oscillatory flow observed with SOFAR floats during the 1978 POLYMODE Local Dynamics Experiment (LDE) [see McWilliams *et al.* (1981) for an overview of the LDE]. Our analysis indicates that this flow had many of the characteristics of a barotropic planetary wave modified by topography. Hence, we term it a "wave" (rather than an eddy) from the outset. A description of this wave is useful in two respects. First, the wave dominated the subthermocline flow during the two-month-long intensive phase of the LDE. The float data provide the best view of its horizontal structure and help provide a

1. Woods Hole Oceanographic Institution, Woods Hole, Massachusetts, 02543, U.S.A.
2. Graduate School of Oceanography, University of Rhode Island, Kingston, Rhode Island, 02881, U.S.A.

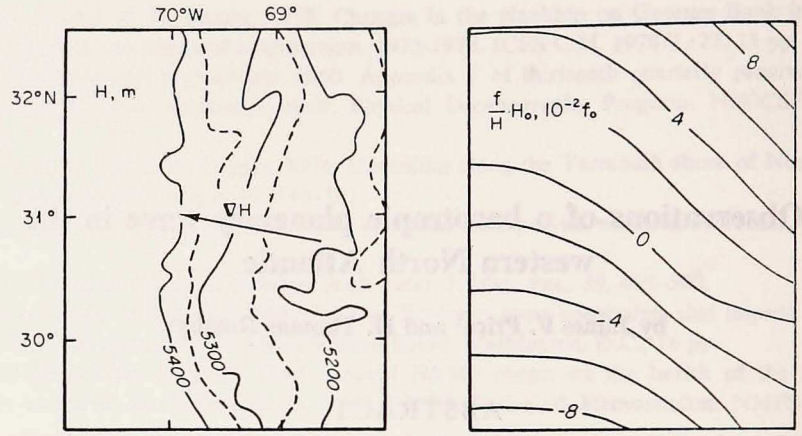

Figure 1. Bottom depth in the LDE region after Pratt (1968) (left), and ambient vorticity $H_o(f/H)$ (right). Our estimate of the large-scale gradient in bottom depth is shown by the vector ∇H, which is scaled so that H changes by 200 m over the length of the vector. The units of ambient vorticity are percent of f_o.

background for analysis and interpretation of other LDE data sets. Secondly, and more generally, these observations are perhaps the most graphic evidence of open-ocean planetary waves acquired to date, and demonstrate the important constraint imposed upon large-scale flows by conservation of potential vorticity.

SOFAR float data are shown in Section 2 as sequences of week-long tracks superimposed on the field of ambient vorticity. This shows both a change of relative vorticity as the flow crosses contours of ambient vorticity and the associated westward phase propagation. The balance of potential vorticity computed in Section 3 is consistent with that of a barotropic planetary wave modified by topography, and the space and time scales computed in Section 4 are consistent with the corresponding dispersion relation. Cautionary remarks on the adequacy of a wave description are in Section 5.

2. Description of the LDE region and the data

Bottom depth H in the central LDE region slopes upward to the east as part of the Bermuda Rise, Figure 1. An estimate of ∇H is required for the potential vorticity analysis and wave dispersion calculation which follow. The quarter wavelength of the wave is 0(100 km) which indicates the scale over which bottom depth should be averaged. East of 70W, where most of the motion occurs, the bottom slope is estimated subjectively to be 150 m/100 km and the mean direction of the isobaths to be 10°T; ∇H is shown in Figure 1 and is given in Table 1. West of 70W, over the Hatteras Abyssal Plain, the bottom slope is much less and ∇H is taken to vanish. The field of ambient vorticity (defined below) was computed at 50 km

Table 1. LDE barotropic planetary/topographic wave parameters.

Parameter	Value	Source
bottom depth	$H_o = 5300$ m	Figure 1
depth gradient	$\nabla H = (-1.45, 0.25) \times 10^{-3}$ east of 70W	
	$= 0$ west of 70W	Figure 1
Coriolis	$f_o = 7.51 \times 10^{-5}$ s^{-1} at 31N	
beta	$\beta = 1.96 \times 10^{-11}$ s^{-1} m^{-1} at 31N	
mean velocity	$\bar{\mathbf{V}} = (-0.02, 0)$ ms^{-1}	Rossby *et al.* (1980)
period	$T = 4.15 \times 10^{6}$ s (48 days)	Same as Fig. 7 w/o Doppler correction
intrinsic period	$T = 5.27 \times 10^{6}$ s (61 days)	Figure 7
wavelength	$\lambda = 340 \times 10^{3}$ m	Figure 7
wave direction	$\theta = 300°$T	Figure 2
amplitude	$\tilde{V} = 0.12$ ms^{-1}	Least squares fit
phase velocity	$C_p = (-0.05, 0.03)$ ms^{-1}	Figure 7
group velocity	$C_g = (0.05, 0)$ ms^{-1}	Figure 8 and dispersion relation

intervals and contoured subjectively, Figure 1. Isolines slope roughly 45° from east-west over the central LDE region, indicating that the variation of H will generally be as important as the variation of the Coriolis parameter f in this region.

As we describe next, the data of Figure 2 demonstrate a barotropic potential vorticity balance,

$$\frac{d}{dt}\left(\frac{\xi + f}{H}\right) = 0 \ , \tag{1}$$

where $\xi = \mathbf{k} \cdot \nabla \times \mathbf{V}$ is the vertical component of relative vorticity. This balance is most apparent in the data in the difference form,

$$\delta\xi \cong -H_o \delta(f/H) \ , \tag{2}$$

where

$$\delta(\ \ ) \equiv \int_{t_1}^{t} \frac{d}{dt}(\ \ )\, d\bar{t}$$

is the change over time *following a given float cluster* (and presumably a water column), and where $(\ \ )_o$ indicates a constant reference value. For the special case of Figure 2, (2) may be further simplified by assigning zero to the $H_o(f/H)$ contour where ξ is observed to vanish. The difference operator may then be dropped to leave

$$R = -A \ , \tag{3}$$

where $R = \xi$, and $A = H_o(f/H)$ are the *r*elative and *a*mbient vorticity which will be given in units of f_o.

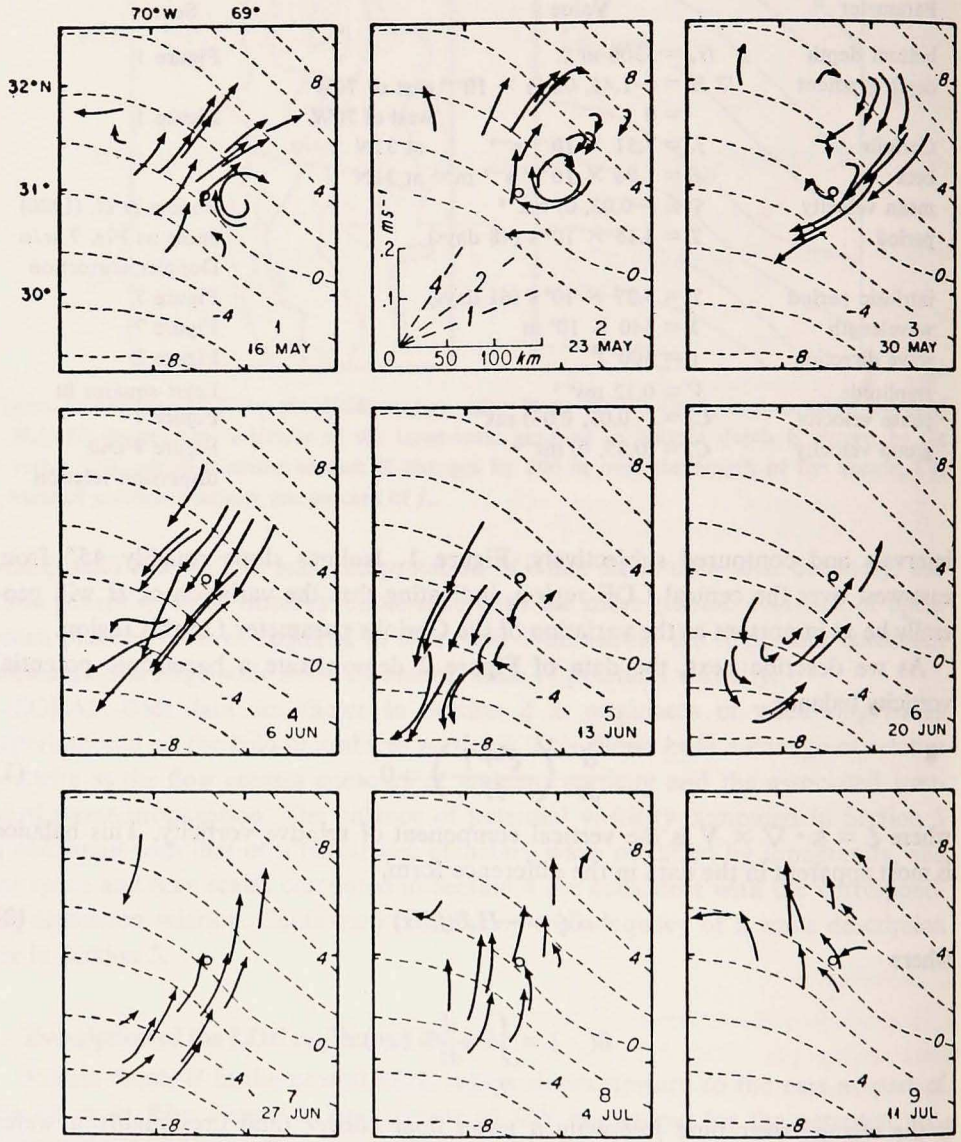

Figure 2. Week-long float trajectories superimposed over ambient vorticity contours. These data have been smoothed with a two-day Gaussian taper to remove tidal and inertial energy. The open circle at 31.0N, 69.5W marks the location of the LDE central mooring. The panel number and the beginning date are noted at lower right of each panel. Speed, distance and a relative vorticity scale are in Panel 2. Units of relative vorticity are percent of f_o (same as the ambient vorticity contours).

During the first week of the experiment, Panel 1 of Figure 2, the large-scale flow of interest here[3] was to the northeast. As the float cluster moved toward larger ambient vorticity, it began to acquire negative relative vorticity as floats on the southeastern side slowed, and then reversed direction, Panel 2. The relative vorticity of the northern half of the cluster (which excludes the small eddy) may be roughly estimated from the scale in Panel 2 as $R \cong -0.03\ f_o$, while $A \cong 0.04\ f_o$. The reversal propagated northwestward through the float cluster, Panel 3, which then accelerated back to the southwest, Panel 4. As the cluster crossed 31N it appears to have given up all relative vorticity, and we have assigned zero to the A contour at 69.5W. The cluster continued southwest to negative values of A, and began to acquire positive R, Panel 5, as again, floats on the southeastern side slowed and then reversed direction. The reversal propagated across the cluster, Panel 6, which then accelerated back to the northeast to begin a second cycle. At the southwest extrema, Panel 6, $R \cong 0.04\ f_o$, while $A \cong -0.04\ f_o$. Thus the gross changes of relative vorticity are qualitatively consistent with barotropic potential vorticity conservation, and there are clear signs of the associated westward phase propagation.

Only 12 of the 18 floats launched at the beginning of the LDE took part in the complete wave cycle described above. Four floats broke away and drifted westward at the time when the cluster was furthest southwest, Panel 5. Two floats that were initially in the northwest corner of the cluster moved off to the west almost from the beginning. One of those floats appeared at times to be roughly a half wavelength westward of the main cluster, Panel 7, but generally did not show a clear phase relation with the main cluster.

A second, somewhat similar oscillation followed. It was not as distinct, and did not involve as many floats (see Spain *et al.*, 1980, for a description of the full data set). The cluster drifted over the Hatteras Abyssal Plain before the second oscillation was completed, and there is no further evidence of the wave.

The heavily instrumented LDE central mooring (Owens *et al.*, 1982) provides a complementary view, Figure 3. During the first three months of the LDE, velocity was approximately uniform from the base of the main thermocline to within a few hundred meters of the bottom; it was somewhat stronger within and above the main thermocline (surface intensified). Velocity was strongly polarized in a plane northeast/southwest and oscillated with a period of $\sim$ 45 days and an amplitude of $\sim 0.13\ \text{ms}^{-1}$. When comparisons may be made, Panels 4 and 8 of Figure 2, the velocity at 1300 m inferred from float observations is very similar to the velocity at 5000 m measured by the current meter. The current meter record clearly shows the temporal intermittency of the wave; two strong oscillations at the beginning of the

[3] Note the small anticyclonic eddy centered on 31N, 69W in Panel 1. This and other small eddies discovered during the LDE will be the topic of future papers by the LDE investigators. This small eddy is "noise" for the purpose here, and will not be discussed except to note when we try to exclude it from analysis of the large-scale flow.

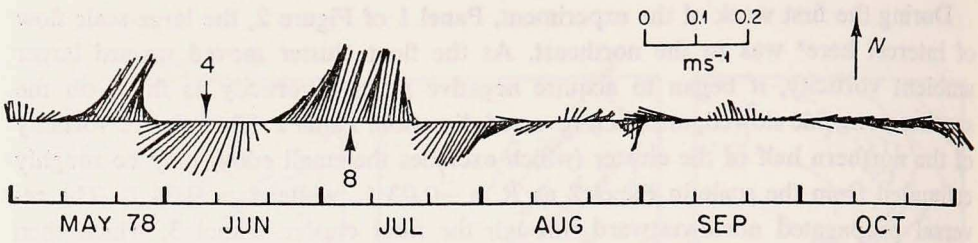

Figure 3. Vector time series of horizontal velocity at 5000 m depth observed at the central mooring, 31N, 69.5W, during the first six months of the LDE. See Owens *et al.* (1982) for the complete record. The arrows marked 4 and 8 denote the times of Panels 4 and 8, Figure 2.

LDE were followed by a several month-long period of much weaker, less strongly polarized velocity.

3. Potential vorticity balance

Here we sharpen our estimate of the potential vorticity balance by performing an objective, quantitative analysis. [See Bryden and Fofonoff (1977) and McWilliams (1976) for detailed analyses of Eulerian potential vorticity balance.] Our intent is not as much to test *whether* potential vorticity was conserved as it is to see *how* potential vorticity was conserved in this case.

Expansion of the right-hand term of (2) gives

$$\delta\xi + \delta f + H_o f_o \delta \frac{1}{H} = 0 \ , \tag{4}$$

or when evaluated from data,

$$R + P + T = \epsilon$$

for the changes in *r*elative, *p*lanetary and *t*opographic vorticity. The residual ϵ could arise from: sampling errors in R, P or T; internal (baroclinic) divergence which is not accounted for in the topographic stretching term, or less likely, departure from an inviscid, unforced balance. P and T are simple functions of position $\mathbf{r} = (x,y)$, (east, north),

$$P = \beta\delta\bar{y}$$

$$T = -\frac{f_o}{H_o}\,\delta\bar{\mathbf{r}} \cdot \nabla H$$

where $\bar{x},\bar{y}$ are the average x,y positions of the float cluster. The first derivatives of velocity required to estimate the relative vorticity, $\xi = \partial v/\partial x - \partial u/\partial y$, are computed by performing a least squares fit of a plane to each velocity component separately (Molinari and Kirwin, 1975; Okubu and Ebbesmeyer, 1976). The error in R is estimated from an identical calculation of divergence $\nabla \cdot \mathbf{V} = \partial u/\partial x + \partial v/\partial y$. It is

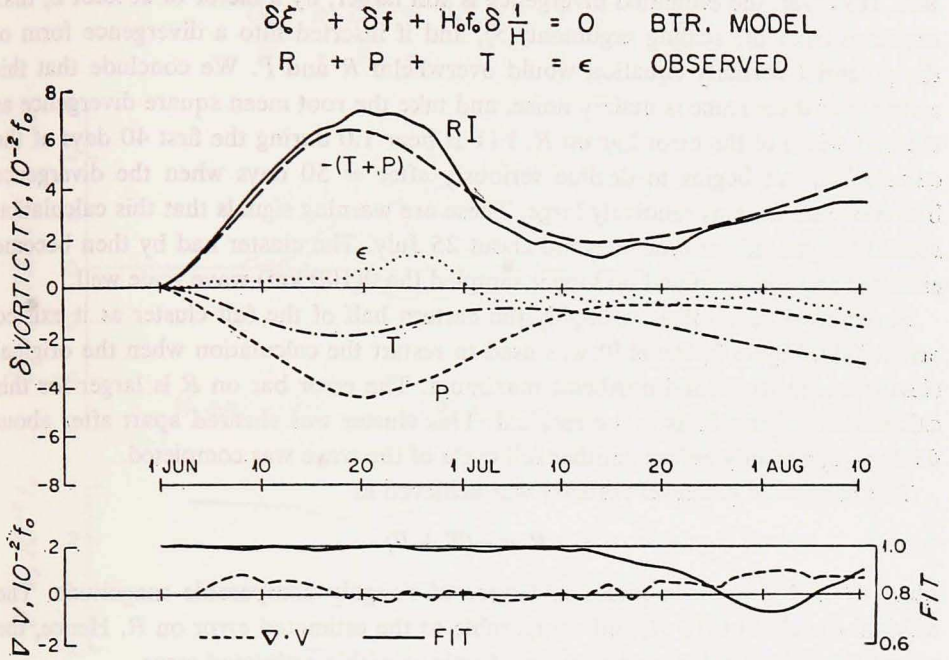

Figure 4. The balance of barotropic potential vorticity computed from a cluster of nine floats (nos. 40-48). Estimates of each term were made at daily intervals.

well known that divergence must be very small in large-scale, quasi-geostrophic motions, typically

$$\frac{\nabla \cdot \mathbf{V}}{\xi} = 0\left(\frac{\xi}{f}\right), \tag{5}$$

where ξ/f is the Rossby number $\cong 0.04$ in this case. The degree to which the estimated divergence meets this severe constraint is a useful measure of the quality of the velocity gradient estimates. The fraction of the observed velocity variance accounted for by the least squares fit, FIT, is also shown. Estimation of the derivatives is suspect when FIT is less than about 0.8.

The calculation is first carried out with a cluster of nine floats which were roughly the northeastern half of the full cluster as seen in Figure 2, Panel 3. This cluster of floats remained fairly compact during a complete cycle of the wave, and were clearly distinct from the small eddy. The initial time $t_1 = 1$ June, when the cluster was at a northeast maximum, Panel 3, and when the relative vorticity was at a negative maximum. The initial *change* in relative vorticity R is thus positive, Figure 4, and the changes in P and T are negative.

The estimated divergence is typically $0.005\ f_o$, while R is typically $0.05\ f_o$, or an order of magnitude larger. This suggests that the velocity derivatives are estimated

well. However, the estimated divergence is still larger, by a factor of at least 2, than expected from the scaling argument (5), and if inserted into a divergence form of the potential vorticity equation would overwhelm R and P. We conclude that this estimate of divergence is mainly noise, and take the root mean square divergence as the half-width of the error bar on R. FIT is near 1.0 during the first 40 days of the calculation, but begins to decline seriously after $\cong$ 50 days when the divergence becomes and remains relatively large. These are warning signals that this calculation should be ignored for times beyond about 25 July. The cluster had by then become enlarged and distorted and no longer sampled the 0(100 km) wave scale well.

A subset of seven floats (roughly the eastern half of the full cluster as it existed on 13 July, Figure 2, Panel 9) was used to restart the calculation when the original cluster was at its second northeast maximum. The error bar on R is larger for this calculation, Figure 5, as is the residual. This cluster was sheared apart after about 45 days, apparently before another full cycle of the wave was completed.

The balance of potential vorticity was achieved as

$$R \cong -(T + P)$$

where T and P were in phase and were of roughly comparable magnitude. The residual ϵ is about 0.15 R, and comparable to the estimated error on R. Hence, the potential vorticity balance appears barotropic to within estimated error.

Other LDE measurements provide independent and certainly more direct evidence that the flow beneath the main thermocline was largely barotropic at this time (McWilliams *et al.*, 1981). As noted in Section 2, the current meter data from 31N, 69.5W at 5000 m depth are very similar to the float velocities at 1300 m when those comparisons may be made. Electromagnetic velocity profiles made in the area also showed strong barotropic flow beneath the main thermocline (Sanford, personal communication). Finally, the hydrographic survey group (Taft and Ebbesmeyer, personal communication) observed that the small eddy moved rapidly across the LDE region (due apparently to advection by the wave described here) though the geostrophic shear integrated from depth up to the level of the eddy was very weak. Hence they too inferred strong barotropic flow beneath the main thermocline.

There is some visual correlation between 1300 m float tracks within the wave and the few available overlying 700 m float tracks (Spain *et al.*, 1980), and there is a similar northwestward propagation evident in the 700 m time- and space-lagged covariance. However, at the 700 m level the wave is somewhat obscured by a strong baroclinic velocity, which Owens *et al.* (1982) refer to as a jet.

4. Time scales, space scales, and wave propagation

To estimate time and space scales of the wave we have computed the time- and space-lagged covariance,

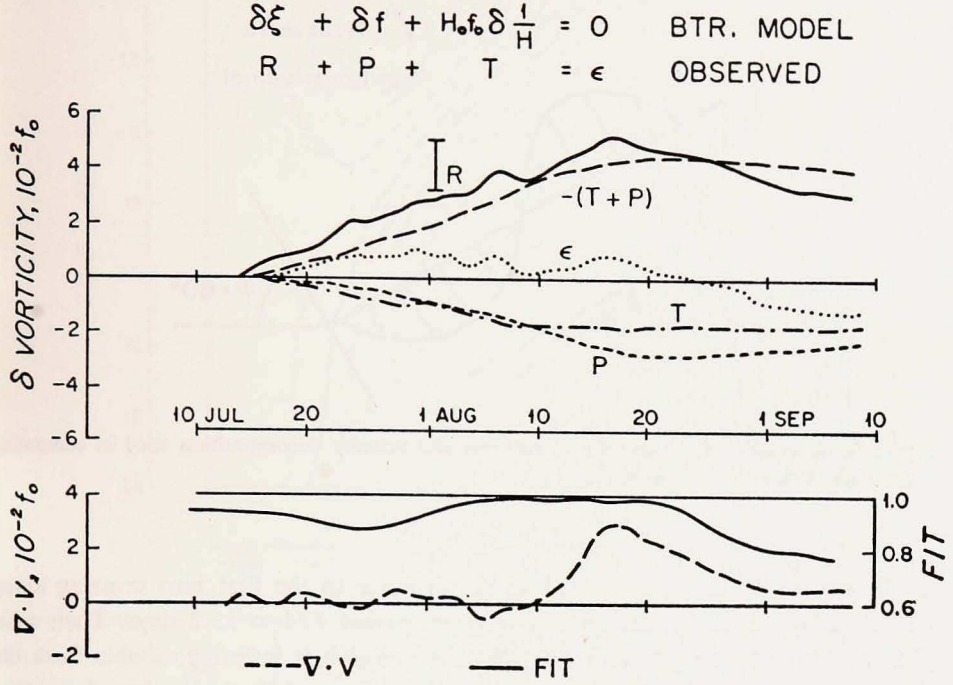

Figure 5. The balance of barotropic potential vorticity computed from a cluster of seven floats (nos. 40-42, 45-48).

$$C_T(\Delta y',\Delta t) = \langle u'(y',t)\, u'(y' + \Delta y' - \bar{v}'\Delta t,\, t + \Delta t) \rangle$$

$$C_L(\Delta y',\Delta t) = \langle v'(y',t)\, v'(y' + \Delta y' - \bar{v}'\Delta t,\, t + \Delta t) \rangle \ .$$

In the discussion of Figure 2 we noted that phase propagated northwestward, in a direction roughly perpendicular to the plane of polarization. This suggests a transverse wave whose plane of polarization is estimated from a principal axes calculation to be 30°/210°T, and whose wave vector is thus estimated to point 300°T. The axes are rotated 60° anticlockwise so that y' is in the direction of the wave vector, Figure 6. Propagation should then be most apparent in the so-called transverse covariance C_T, while the longitudinal covariance C_L should vanish. Additionally, the observed time- and space-averaged mean velocity $\bar{\mathbf{V}} = (-0.02, 0)$ ms^{-1} (Rossby *et al.*, 1980) is subtracted from the rotated velocity components u',v', and more importantly from the positions to remove Doppler shifting. Whether this "mean velocity" is appropriate for this particular time and place is problematic and we comment below on the effect of Doppler correcting.

The transverse covariance, Figure 7, shows a striking slope of isolines indicative of propagation toward the northwest at a rate $\cong$ 0.06 ms^{-1}. The quarter wave-

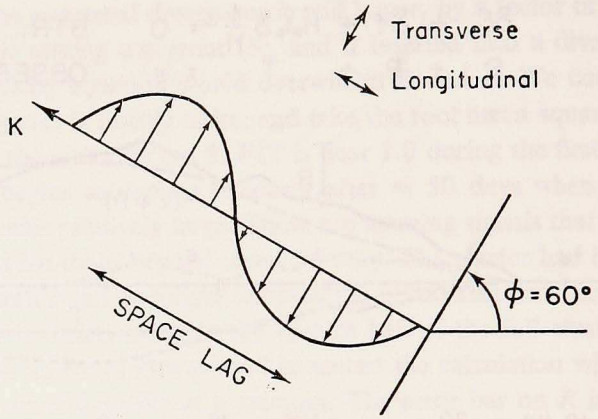

Figure 6. Schematic of the coordinate rotation and velocity decomposition used in computing time- and space-lagged covariance.

length $\lambda/4 = 85$ km is estimated as the distance to the first zero crossing along zero time lag; similarly, the quarter intrinsic period $T/4 = 15.2$ days. Their ratio gives a phase speed $C_p = \lambda/T = 0.065$ ms^{-1} which is indistinguishable from the slope of isolines. The longitudinal covariance shows no obvious signal, and as anticipated, has much smaller amplitude.

These estimates of wavelength and period may be used to check whether this wave propagates the way expected of a plane, barotropic planetary wave over the LDE topography. Plane waves with phase $\sim (kx + ly - \omega t)$ satisfy a dispersion relation (LeBlond and Mysak, 1978)

$$\omega = \frac{-k\left(\beta - \frac{f_o}{H_o}\frac{\partial H}{\partial y}\right) - l\,\frac{f_o}{H_o}\frac{\partial H}{\partial x}}{k^2 + l^2}, \tag{6}$$

where we have ignored divergence and thus the very long barotropic wave. Given the observed intrinsic frequency ω and known bottom depth gradient (Table 1), the slowness curve, Figure 8, is the terminus of all possible wave vector solutions to (6). The thin lines surrounding the slowness curve and the wave vector are error bounds estimated from a least squares fit of a plane wave to the observed velocity field (discussed in Section 5). The error bounds are taken to be the values of ω, $\mathbf{K}$ for which the fit is 0.95 of the optimum fit; $\pm$ 0.16 of ω, $\pm$ 10° in direction of $\mathbf{K}$, and $\pm$ 0.28 of λ. The optimum values of ω and $\mathbf{K}$ direction are quite similar to those deduced from Figure 7, but the optimum λ is somewhat less, $\cong$ 300 km. The large uncertainty on λ is probably a result of the rather narrow range of spatial lags sampled by the float cluster.

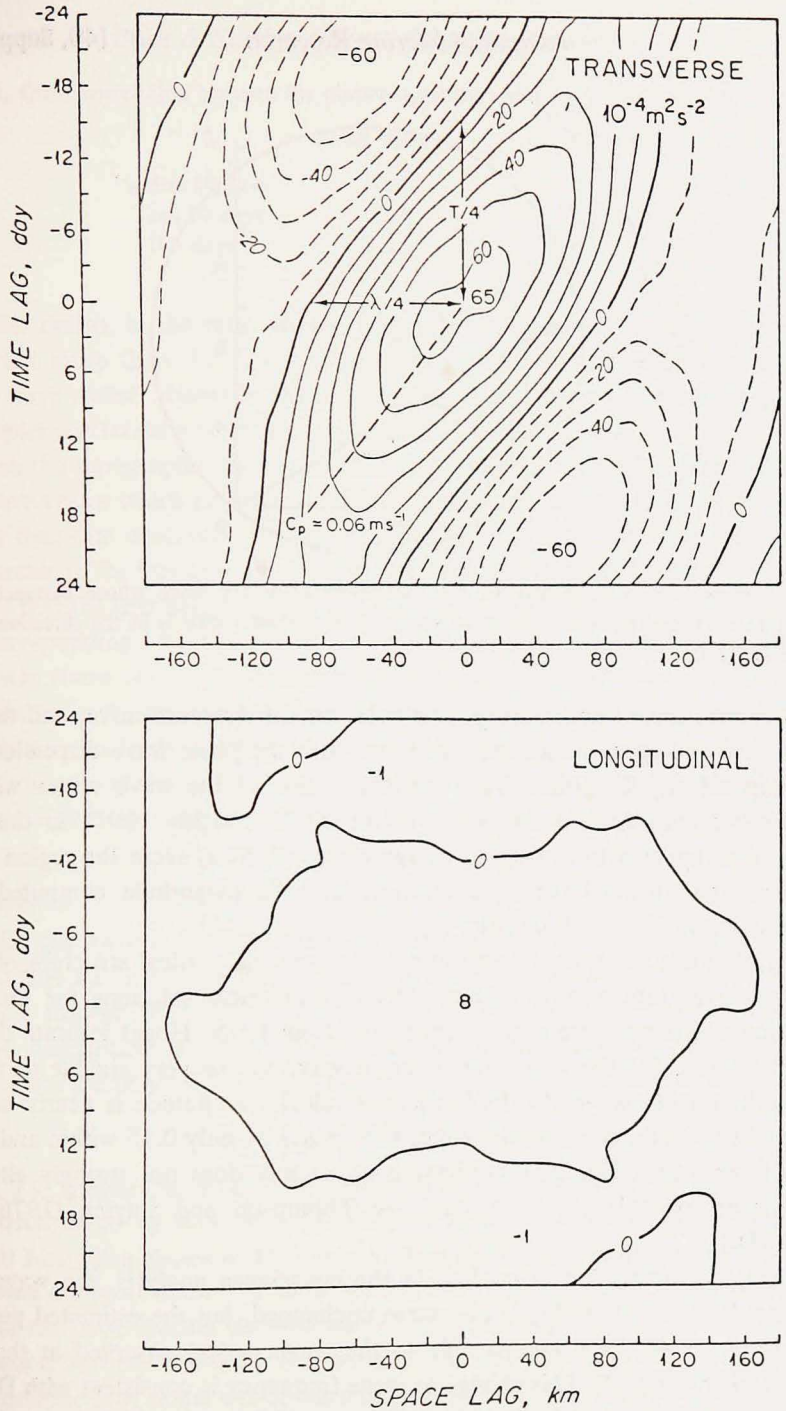

Figure 7. Time- and space-lagged covariance computed from float velocities. The upper panel is computed from the transverse velocity component, the lower panel from the longitudinal component. The dashed line in the transverse covariance is a subjective estimate of the mean slope of the isolines and indicates propagation toward 300°T at 0.06 ms^{-1}.

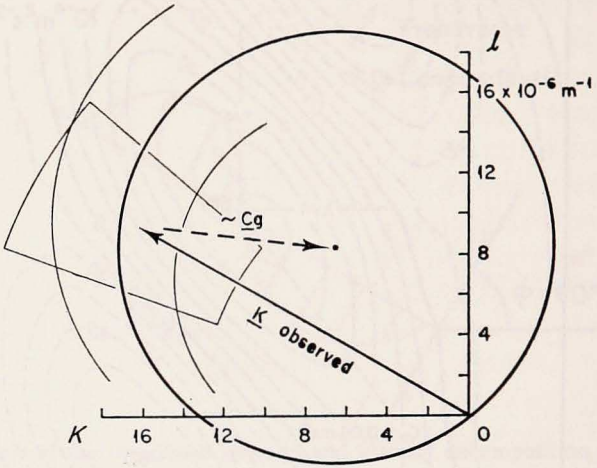

Figure 8. Slowness curve computed for the barotropic planetary wave whose parameters are given in Table 1, and the observed wave vector. The dashed vector is in the direction of the group velocity $\mathbf{C}_g$.

The observed wave vector nearly terminates on the slowness curve, and thus the observed time and space scales are consistent with the plane wave dispersion relation. Group velocity $\mathbf{C}_g$ points from the intersection of the wave vector with the slowness curve back toward the center of the circle, roughly 100°T in this case. The wave thus appears to propagate energy eastward, away from the region of the Gulf Stream and toward the gyre interior. The $\mathbf{C}_g$ magnitude computed from the dispersion relation is $\cong 0.05$ ms^{-1}.

Stratification can alter the dispersion relation and the vertical structure of planetary waves over topography (Rhines, 1970). Numerical solutions for the LDE stratification and these wave parameters (carried out by N. Hogg) indicate that the gravest mode has, for the same frequency, a wave vector very similar to that of the simple barotropic wave (6). Its horizontal velocity amplitude is nearly uniform with depth beneath the main thermocline, and decays by only 0.15 within and above the main thermocline. Hence, stratification apparently does not strongly alter this wave. [For an example where it does, see Thompson and Luyten (1976), and Hogg (1981).]

If no Doppler correction is applied in the covariance analysis, the wavelength estimate made at zero time lag is of course unchanged, but the estimated period is reduced to about 48 days, comparable to the wave period observed at the LDE central mooring, Figure 3. This change in wave frequency is consistent with Doppler shifting given the observed $\mathbf{K}$, i.e., $\Delta\omega/|\mathbf{K}| = -.018$ ms^{-1}, which is roughly the component of the mean velocity in the direction of $\mathbf{K}$. Hence, a Doppler shift may have been observed. The slowness curve for the uncorrected, higher frequency has

Table 2. Cross-correlation between the observed velocity and the velocity of the inferred wave.

	all floats	w/o small eddy
first 90 days	0.72	0.77
last 90 days	−0.07	−0.09
180 days	0.47	0.48

a smaller radius, in the ratio 48/61, and falls inside the observed wave vector by somewhat more than the Doppler corrected slowness curve falls beyond the observed wave vector. However, the dispersion relation test is not particularly sensitive to Doppler correction given the uncertainties of ω and **K**.

When the topographic terms are excluded from the dispersion relation, the solution wave vector which points toward 300°T then has $\lambda = 480$ km, or roughly 40% greater than that observed. The topographic effect in the dispersion relation is thus comparable to the topographic effect in the potential vorticity balance.

Note that the first negative lobe of C_T at $\Delta t = T/2$, $\Delta y' = 0$ is much deeper than the corresponding lobe at $\Delta t = 0$, $\Delta y' = \lambda/2$. At face value, this suggests that the wave was more oscillatory temporally than spatially. However, it is likely more attributable to the nonstationarity of the wave and the float sampling scheme. The float cluster was fairly compact in the northwest/southeast direction during the first several months of the LDE when the wave was present; large spatial lags were not sampled until later in the experiment when the wave was evidently not present.

5. Remarks

While the wave is perhaps the most impressive feature of the large scale, subthermocline LDE velocity field[4], we emphasize that it falls well short of being a complete account of that field. One simple objective measure of the adequacy of a wave description is given by the cross-correlation between the inferred wave velocity and the observed velocity. We may write the wave's transverse velocity as

$$V = \tilde{V} \cos [\, | \mathbf{K} | \, y + \omega(t - t_o)] \ , \tag{7}$$

where y is antiparallel to **K**, and the origin is 31N, 69.5W. The magnitude $\tilde{V}$ has been determined by least squares analysis to be 0.12 ms^{-1}; the phase constant $t_o = 10$ June. The choice of $\tilde{V}$ does not affect the cross-correlation though of course the phase constant does. The data set has been broken down by time, and by the scale of the flow. During the first half of the float experiment (90 days) the cross-correlation between the observed velocity and the wave velocity is 0.72, Table 2. If we exclude four floats which were initially involved in the small eddy and which

[4] The mass transport carried in a half wavelength may be estimated as $\tilde{V} H \lambda 2/\pi \cong 70 \times 10^6$ m^{3}s^{-1}, where $\tilde{V} = 0.12$ ms^{-1} is the velocity amplitude. This transport is comparable to that of the Gulf Stream at this latitude.

clearly cannot be described by (7), then the cross-correlation is slightly higher, 0.77. Hence, the wave accounts for most, but by no means all, of the large-scale velocity observed by the floats during the first half of the LDE. If instead we use only data from the second half of the experiment, then the cross-correlation is −0.09, or essentially zero. Again, there is no evidence that the wave persisted for more than two cycles beyond the start of the LDE.

Westward phase propagation of open-ocean mesoscale eddies has been widely reported [see the reviews by LeBlond and Mysak (1978) and Wunsch (1981)]. However, few if any of the previous observations are as simply and clearly wavelike as this one. For example, Freeland *et al.* (1975) found that westward propagation, but not necessarily a dispersion relation, was a persistent feature of the MODE velocity field which they suspected to be moderately nonlinear (particle speeds > phase speeds). In this case, we observe westward propagation of a transient, at least approximately linear wave. Wave fits to the mesoscale eddies observed in the POLYGON (McWilliams and Robinson, 1974) and MODE experiments (McWilliams and Flierl, 1976) required a superposition of several barotropic and baroclinic plane waves to match the cellular structure of the observed velocity field. This wave is by comparison long crested; Rossby *et al.* (1980) found that the (conventional) longitudinal correlation in the plane of polarization is 0.8 at 120 km separation (the zero crossing was not sampled). Hence, a single plane wave can be a plausible description. Dispersion and nonlinear effects, troublesome features of a wave superposition, thus do not arise here.

Our data set provides a detailed look at some of the (spatially) local properties of the wave, but probably cannot provide direct answers to important questions on its global dynamics, e.g., energy sources and sinks. Evidence from a variety of sources, including field observations (Schmitz, 1978) and numerical models (Holland, 1978), suggests that the Gulf Stream is the major source of barotropic eddy energy found in the LDE region. The (locally) eastward pointing group velocity of Figure 8 is consistent with direct forcing by a meandering Gulf Stream [as envisioned by Pedlosky (1977) and Harrison and Robinson (1979)], but other less direct mechanisms are also possible. Rhines (1977) has shown that intense baroclinic eddies evolve toward barotropy. The occurrence of relatively intense thermocline-depth currents [baroclinic jet of Owens *et al.* (1982)] at the beginning of the LDE hints at this latter mechanism.

Acknowledgments. We credit the success of our field experiment to the efforts of the SOFAR float operations group at Woods Hole Oceanographic Institution and the SOFAR float tracking group at the University of Rhode Island. We must especially mention Dr. A. Bradley who designed and built the Autonomous Listening Station, Mr. D. Webb who supervised float preparation and deployment assisted by Mr. J. Valdes and Mr. R. Lavoie, and Ms. D. Spain who supervised the data reduction assisted by Mr. C. Polloni and Ms. R. O'Gara. Funding for the POLYMODE SOFAR float program was provided by the International Decade of Ocean Ex-

ploration office of the National Science Foundation through grant OCE78-18662-A02. Thanks go to Drs. B. Owens, J. Luyten, and H. Bryden for providing their current meter data in advance of their own publication, and to Drs. J. McWilliams, R. Hall and N. Hogg for their helpful comments on this manuscript. Contribution number 4713 of the Woods Hole Oceanographic Institution and number 152 of the Mid-Ocean Dynamics Experiment (POLYMODE).

REFERENCES

Bryden, H. L. and N. P. Fofonoff. 1977. Horizontal divergence and vorticity estimates from velocity and temperature measurements in the MODE region. J. Phys. Oceanogr., *7*, 329–337.

Freeland, H. J., P. B. Rhines and H. T. Rossby. 1975. Statistical observations of the trajectories of neutrally buoyant floats in the North Atlantic. J. Mar Res., *33*, 383–404.

Harrison, D. E. and A. R. Robinson. 1979. Boundary-forced planetary waves: A simple model mid-ocean response to strong current variability. J. Phys. Oceanogr., *9*, 919–929.

Hogg, N. 1981. Topographic waves along 70W on the Continental Rise. J. Mar. Res., *39*, 627–649.

Holland, W. R. 1978. The role of mesoscale eddies in the general circulation of the ocean-numerical experiments using a wind-driven quasi-geostrophic model. J. Phys. Oceanogr., *8*, 363–392.

LeBlond, P. H. and L. D. Mysak. 1978. Waves in the Ocean. Elsevier Pub. Co., Amsterdam, 602 pp.

McWilliams, J. C. 1976. Maps from the Mid-Ocean Dynamics Experiment II. Potential vorticity and its conservation. J. Phys. Oceanogr., *6*, 828–846.

McWilliams, J. C. and G. R. Flierl. 1976. Optimal, quasi-geostrophic wave analyses of MODE array data. Deep-Sea Res., *23*, 285–300.

McWilliams, J. C. and the LDE Group. 1981. The local dynamics of eddies in the Western North Atlantic, *in* Eddies Marine Science, A. R. Robinson, ed.

McWilliams, J. C. and A. R. Robinson. 1974. A wave analysis of the Polygon array in the tropical Atlantic. Deep-Sea Res., *21*, 359–368.

Molinari, R. and A. D. Kirwin, Jr. 1975. Calculation of differential kinematic properties from Lagrangian observations in the western Caribbean Sea. J. Phys. Oceanogr., *5*, 483–491.

Okubo, A. and C. C. Ebbesmeyer. 1976. Determination of vorticity, divergence and deformation rates from analysis of drogue observations. Deep-Sea Res., *23*, 349–352.

Owens, W. B., J. R. Luyten and H. C. Bryden. 1982. Moored velocity measurements during the POLYMODE Local Dynamics Experiment. J. Mar. Res., *40* (Supp.), 509–524.

Pedlosky, J. 1977. On the radiation of meso-scale energy in the mid-ocean. Deep-Sea Res., *24*, 591–600.

Pratt, R. M. 1968. Atlantic Continental Shelf and slope of the United States—physiography and sediments of the deep-sea basin. Geological Survey Professional Paper 529-B, U.S. Government Printing Office, Plate I.

Rhines, P. B. 1970. Edge-, bottom- and Rossby waves in a rotating stratified fluid. Geophys. Fluid Dyn., *1*, 273–302.

—— 1977. The dynamics of unsteady currents, *in* The Sea, Vol. 6, E. D. Goldberg, ed., John Wiley and Sons, Inc., New York, 189–318.

Rossby, H. T., J. F. Price and D. C. Webb. 1980. The spatial and temporal evolution of a cluster of SOFAR floats in the POLYMODE Local Dynamics Experiment, (unpublished manuscript).

Schmitz, W. J., Jr. 1978. Observations of the vertical distribution of low frequency kinetic energy in the western North Atlantic. J. Mar. Res., *36*, 295–310.

Spain, D. L., R. M. O'Gara and H. T. Rossby. 1980. SOFAR float data report of the POLYMODE Local Dynamics Experiment. University of Rhode Island, TR No. 80-1, 200 pp.

Thompson, R. O. R. Y. and J. R. Luyten. 1976. Evidence for bottom-trapped topographic Rossby waves from single moorings. Deep-Sea Res., *23*, 629–635.

Wunsch, C. 1981. Low frequency variability of the sea, *in* Evolution of Physical Oceanography, B. A. Warren and C. Wunsch, eds., The MIT Press, Cambridge, Massachusetts, 623 pp.

Received: *25 November, 1980;* revised: *4 January, 1982.*